JOURNAL OF MATERIALS SCIENCE **38** (2003) 3019–3027

A multi-scale framework for effective elastic properties of porous materials

LIANGSHENG WANG, KEVIN K. TSENG*
Department of Civil and Environmental Engineering, Vanderbilt University, VU Station B 351831, Nashville, TN 37235, USA
E-mail: Liangsheng.Wang@Vanderbilt.edu
E-mail: Kevin.Tseng@Vanderbilt.Edu

This paper presents a statistical micromechanics-based multi-scale material modeling framework to predict the effective elastic moduli of porous materials. The present formulation differs from most of the existing theoretical models in that the interaction effects among the pores are directly accounted for by considering the pair-wise interaction and the statistical information of pore distribution is included by applying the ensemble volume averaging process. The theory of average fields is employed to derive the stress and strain concentration factor tensors that relate the local average fields to the global averages. Closed-form and analytical explicit expressions for the effective elastic moduli of porous materials are obtained in terms of the mechanical properties of the matrix material and porosity. The dependence of effective elastic properties on the porosity is investigated. Comparison of our theoretical prediction with the results of the published experimental data and other existing theoretical models is performed to illustrate the predictive capability of the proposed framework for porous materials. © *2003 Kluwer Academic Publishers*

1. Introduction

Porous materials have been used in a wide range of applications in various engineering areas from ceramics to porous shape memory alloys. In order to utilize porous materials effectively, it is desired to know their mechanical behavior as a function of porosity. A number of empirical equations and theoretical models have been developed for the effective elastic properties of porous materials. Though empirical equations can provide accurate descriptions of experimental data, theoretical models having rigorous connection with the microstructure are usually more predictive and interpretive.

The prediction and estimation of the effective mechanical properties of porous materials are of great interest to researchers and engineers in the science and engineering disciplines. There are many theoretical methods in the literature to tackle this class of problems [1]. Most of these existing theoretical models have been developed by assuming the porous material as a special case of a two-phase composite and extending the results of a representative two-phase element to the continuum material. The unit cell technique is used to derive the effective elastic moduli by assuming a periodic distribution of pores [2]. The representative volume element technique predicts the averaged macroscopic elastic properties of the porous material with random distribution of pores. In this technique, the effective properties of a heterogeneous porous material are obtained by some volume- and ensemble-averaging processes over a representative volume element (RVE) featuring a mesoscopic length scale which is much larger than the characteristic length scale of inclusions but smaller than the characteristic length scale of a macroscopic specimen. This technique includes the self-consistent method [3, 4], the differential method [5] and the Mori-Tanaka method [6]. Qidwai *et al.* [2] investigated the elastic and thermomechanical behavior of porous shape memory alloys using both the unit cell and representative volume element techniques. Other theoretical methods include the minimum solid area model [7] and the generalized method of cells [8].

In this paper, we propose to use a statistical micromechanical model with closed-form and analytical explicit expressions to describe the effective elastic moduli of porous materials. This approach differs from other existing theoretical models in that the interaction effects among pores are accounted for by considering the pair-wise interaction between two pores and the statistical distribution of pores is taken into account by applying the ensemble-volume averaging process. To simplify the derivation, all pores are assumed spherical in shape and equal in size. The pores are distributed randomly among the matrix material. Accordingly, a microscopically heterogeneous porous material can be equivalently replaced by a macroscopically homogeneous continuum medium with properly defined effective properties. Nevertheless, the proposed

*Author to whom all correspondence should be addressed.

framework is capable of modeling more general problems including the variation of pore size, shape, and the distribution.

Since the pores are assumed to be distributed randomly among the matrix, it is impractical to consider only a given realization of the distribution of pores. Furthermore, the pores could be close to each other in the case of moderate to high concentrations of pores in the porous material. The interaction effects among the pores are therefore an important factor when considering the macroscopic properties of the porous material. However, considering the effects of interaction among all the pores is intractable due to the large number of pores typically present in the porous material. In this paper, the effect of interaction between two pores is calculated analytically at the microscopic level. The pair-wise interaction solution is then averaged among the statistical space to account for the inhomogeneity of the porous material. This leads to approximate yet closed-form analytical results.

This paper is organized as follows. In Section 2, we first consider a linear elastic two-phase composite containing randomly located spherical inclusions. The formulation starts by applying the theory of average fields to establish the relations between the effective elastic moduli and the concentration factor tensors. The concept of eigenstrain via the Eshelby's equivalence principle is introduced to solve the problem of two-sphere interaction in an infinite elastic matrix. Approximate closed-form solutions are derived for this pairwise interaction problem. Based on the solutions, an ensemble average is performed to account for the statistical distribution of the inclusions among the matrix material. The stress and strain concentration factor tensors are identified based on the governing ensemble-volume averaged field equation that relates the macroscopic strain, the uniform remote strain and the average eigenstrain, and the effective elastic moduli for a two-phase composite are derived. Finally, explicit closed forms for the effective elastic moduli of porous materials are derived in terms of the mechanical properties of the matrix material and porosity. To assess the accuracy of the proposed framework, comparisons between our predictions and the results of the published experimental data and other existing theoretical models are given in Section 3.

2. Effective elastic behavior of porous materials

In this section, we first attempt to construct an accurate estimation of the effective elastic moduli of a two-phase composite system containing randomly located spherical inclusions based on the theory of average fields, the proposed approximate pairwise interaction solutions and the ensemble-volume averaging process. Based on the solutions, closed-form and analytical explicit expressions for the effective elastic moduli of porous materials are then derived in terms of the mechanical properties of the matrix material and porosity.

For the simplicity of presentation and mathematical operation, we assume that the material properties for both the matrix phase and the inclusion phase in a two-phase composite system are isotropic and the loading at any local material point remains within the elastic limit. It is further assumed that the inclusions do not intersect each other and the material properties of both phases remain unchanged for the loading considered. Nevertheless, the framework that is proposed in this paper is valid for the general composite system with any arbitrary material property for the constituent phase.

2.1. Relations between effective elastic moduli and concentration factor tensors

For a two-phase composite consisting of an elastic matrix (phase 0) and randomly dispersed elastic spherical inclusions (phase 1), the relations between the stress σ and strain ϵ at any point x in the α-phase ($\alpha = 0$ or 1) are governed by

$$\boldsymbol{\sigma}_\alpha(\mathbf{x}) = \mathbf{C}_\alpha : \boldsymbol{\epsilon}_\alpha(\mathbf{x}) \tag{1}$$

$$\boldsymbol{\epsilon}_\alpha(\mathbf{x}) = \mathbf{D}_\alpha : \boldsymbol{\sigma}_\alpha(\mathbf{x}) \tag{2}$$

where the operator: denotes the tensor contraction, and $\mathbf{C}_\alpha$ and $\mathbf{D}_\alpha$ are the elastic stiffness and compliance tensors for α-phase, respectively.

By taking the volume average of Equations 1 and 2 over the sub-domain occupied by the α-phase, we obtained the following two equations that relate the local average stress and strain fields

$$\bar{\boldsymbol{\sigma}}_\alpha = \mathbf{C}_\alpha : \bar{\boldsymbol{\epsilon}}_\alpha \tag{3}$$

$$\bar{\boldsymbol{\epsilon}}_\alpha = \mathbf{D}_\alpha : \bar{\boldsymbol{\sigma}}_\alpha \tag{4}$$

where an over-bar represents the volume average of the corresponding quantity.

Similarly, the macroscopic elastic properties can be expressed by the following equations through the global effective elastic moduli

$$\bar{\boldsymbol{\sigma}} = \mathbf{C}_* : \bar{\boldsymbol{\epsilon}} \tag{5}$$

$$\bar{\boldsymbol{\epsilon}} = \mathbf{D}_* : \bar{\boldsymbol{\sigma}} \tag{6}$$

where $\mathbf{C}_*$ and $\mathbf{D}_*$ are the global effective elastic stiffness and compliance tensors, respectively.

Due to the high degree of complexity of the arbitrary geometry and concentration of the inclusions, the determination of the exact internal local stress or strain field in a composite system is in general formidable. In many applications, the average of the field provides a tractable avenue based on the volume-averaged quantities than the actual local solutions. A method based on the so called stress and strain concentration factors was introduced by Hill [9] and later extended by Dvorak [10] to address the effective properties of composite materials.

In physical sense, the concentration factor defines the relationship between the local field and the average of the global field. In the case of the stress field, the stress at any local point for a specific material phase is related to the average stress for the global composite system via the stress concentration factor. If only the average of the local stress field is required, upon averaging over

the local material phase, we can obtain the following relationship

$$\bar{\boldsymbol{\sigma}}_\alpha = \mathbf{B}_\alpha : \bar{\boldsymbol{\sigma}} \tag{7}$$

where the fourth rank tensor $\mathbf{B}_\alpha$ is the volume averaged stress concentration factor tensor for phase α.

Similar definition is made for the strain field

$$\bar{\boldsymbol{\epsilon}}_\alpha = \mathbf{A}_\alpha : \bar{\boldsymbol{\epsilon}} \tag{8}$$

in which $\mathbf{A}_\alpha$ is the volume averaged strain concentration factor tensor for phase α.

Since the two material phases are assumed not to overlap each other, the averaging process at the global scale can be separated into two parts—one for each phase. Therefore, the following two equations can be obtained

$$\bar{\boldsymbol{\sigma}} = \phi_0 \bar{\boldsymbol{\sigma}}_0 + \phi_1 \bar{\boldsymbol{\sigma}}_1 \tag{9}$$

$$\bar{\boldsymbol{\epsilon}} = \phi_0 \bar{\boldsymbol{\epsilon}}_0 + \phi_1 \bar{\boldsymbol{\epsilon}}_1 \tag{10}$$

where ϕ_α denotes the α-phase volume fraction.

With Equations 7 and 8, the relationship between the concentration factors for the two phases can be written as

$$\phi_0 \mathbf{B}_0 + \phi_1 \mathbf{B}_1 = \mathbf{I} \tag{11}$$

$$\phi_0 \mathbf{A}_0 + \phi_1 \mathbf{A}_1 = \mathbf{I} \tag{12}$$

where $\mathbf{I}$ is the fourth rank identity tensor.

Consequently, from Equations 3–10, the global effective elastic moduli are expressed in terms of the volume fractions, the elastic moduli of the constituent phases, and the concentration factor tensors as shown in the following two equations

$$\mathbf{C}_* = \phi_0 \mathbf{C}_0 \cdot \mathbf{A}_0 + \phi_1 \mathbf{C}_1 \cdot \mathbf{A}_1 \tag{13}$$

$$\mathbf{D}_* = \phi_0 \mathbf{D}_0 \cdot \mathbf{B}_0 + \phi_1 \mathbf{D}_1 \cdot \mathbf{B}_1 \tag{14}$$

More concise and convenient forms which depend on quantities related to a single material phase can be derived with the help of Equations 11 and 12 ($\alpha \neq \beta$):

$$\mathbf{C}_* = \mathbf{C}_\alpha + \phi_\beta (\mathbf{C}_\beta - \mathbf{C}_\alpha) \cdot \mathbf{A}_\beta \tag{15}$$

$$\mathbf{D}_* = \mathbf{D}_\alpha + \phi_\beta (\mathbf{D}_\beta - \mathbf{D}_\alpha) \cdot \mathbf{B}_\beta \tag{16}$$

From Equations 15 and 16, the global effective elastic moduli for a two-phase composite system can be obtained provided that the stress or strain concentration factor tensor is available.

2.2. Approximate solutions of two-sphere interaction problem

Let us consider the problem of two spherical inclusions embedded firmly in an infinite elastic solid subjected to a far field loading. For simplicity, it is assumed that the two spherical inclusions are of the same size and their

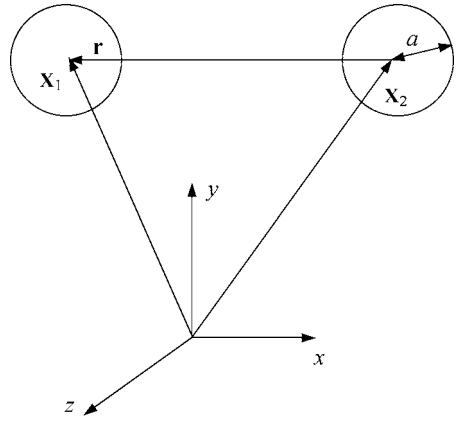

Figure 1 Schematic diagram of two-sphere interaction problem.

radius is denoted as a. As shown in Fig. 1, the locations for the centers of spherical inclusion 1 and 2 are denoted as $\mathbf{x}_1$ and $\mathbf{x}_2$, respectively. There are two material phases in this problem. Phase 0 and 1 denotes the matrix and inclusion phase, respectively. Furthermore, Ω_1 and Ω_2 represent the domain inside of inclusion 1 and 2, respectively. The vector $\mathbf{r}$ denotes the relative position between the two centers.

When applying the Eshelby's equivalence principle to the inclusion problem without considering the effects of inter-inclusion interaction, the equation for determining the non-interacting solution for the eigenstrain in an inclusion, denoted by $\boldsymbol{\epsilon}^{*0}$, which had been proved to be constant throughout the entire spherical region, can be written as

$$-\mathbf{A} : \boldsymbol{\epsilon}^{*0} = \boldsymbol{\epsilon}^0 + \mathbf{S} : \boldsymbol{\epsilon}^{*0} \tag{17}$$

where

$$\mathbf{A} = (\mathbf{C}_1 - \mathbf{C}_0)^{-1} \cdot \mathbf{C}_0 \tag{18}$$

in which $\mathbf{C}_0$ and $\mathbf{C}_1$ are the stiffness tensor for the matrix and inclusion phase, respectively.

In Equation 17, $\mathbf{S}$ is the Eshelby's tensor for a spherical inclusion and is defined as

$$\mathbf{S} = \int_\Omega \mathbf{G}(\mathbf{x} - \mathbf{x}')\, d\mathbf{x}', \quad \mathbf{x} \in \Omega \tag{19}$$

where the tensor $\mathbf{G}(\mathbf{x} - \mathbf{x}')$ is the Green's function for elasticity and is defined by the following equation

$$\boldsymbol{\epsilon}(\mathbf{x}) = \int_\Omega \mathbf{G}(\mathbf{x} - \mathbf{x}') : \boldsymbol{\epsilon}^*(\mathbf{x}')\, d\mathbf{x}' \tag{20}$$

in which $\boldsymbol{\epsilon}(\mathbf{x})$ denotes the strain tensor at the location $\mathbf{x}$, $\boldsymbol{\epsilon}^*(\mathbf{x})$ is the tensor of eigenstrain.

The explicit form for the tensor components of $\mathbf{S}$ can be found in [11] for the spherical inclusion considered in the present study. The Eshelby's tensor for other shapes of inclusion can be found in [11].

By taking into account the effects of inter-inclusion interaction within the present two-sphere context, the integral equation governing the distributed eigenstrain

can be expressed as

$$-\mathbf{A}:\boldsymbol{\epsilon}^*(\mathbf{x}) = \boldsymbol{\epsilon}^0 + \int_{\Omega_i} \mathbf{G}(\mathbf{x}-\mathbf{x}'):\boldsymbol{\epsilon}^*(\mathbf{x}')\,d\mathbf{x}' + \int_{\Omega_j} \mathbf{G}(\mathbf{x}-\mathbf{x}'):\boldsymbol{\epsilon}^*(\mathbf{x}')\,d\mathbf{x}' \quad (21)$$

where the last term in the right-hand side of Equation 21 represents the interaction effect due to the other sphere.

By subtracting the non-interacting solution (17) from (21), the effect of inter-inclusion interaction can be found by solving the following integral equation

$$-\mathbf{A}:\mathbf{d}^*(\mathbf{x}) = \int_{\Omega_j} \mathbf{G}(\mathbf{x}-\mathbf{x}')\,d\mathbf{x}':\boldsymbol{\epsilon}^{*0} + \int_{\Omega_i} \mathbf{G}(\mathbf{x}-\mathbf{x}'):\mathbf{d}^*(\mathbf{x}')\,d\mathbf{x}' + \int_{\Omega_j} \mathbf{G}(\mathbf{x}-\mathbf{x}'):\mathbf{d}^*(\mathbf{x}')\,d\mathbf{x}' \quad (22)$$

where

$$\mathbf{d}^*(\mathbf{x}) = \boldsymbol{\epsilon}^*(\mathbf{x}) - \boldsymbol{\epsilon}^{*0} \quad (23)$$

Following the procedure detailed in [12], the following equation can be obtained after dropping the higher order terms for the parameter $\rho = \frac{a}{r}$ and r is the spacing between the centers of two spheres:

$$-\mathbf{A}:\mathbf{d}^* = \mathbf{G}^2(\mathbf{x_1}-\mathbf{x_2}):\boldsymbol{\epsilon}^{*0} + \mathbf{S}:\mathbf{d}^* + \mathbf{G}^1(\mathbf{x_1}-\mathbf{x_2}):\mathbf{d}^* \quad (24)$$

The tensors in Equation 24 are defined as

$$\mathbf{d}^* = \frac{1}{\Omega}\int_{\Omega} \mathbf{d}^*(\mathbf{x})\,d\mathbf{x} \quad (25)$$

$$\mathbf{G}^1(\mathbf{x}_1-\mathbf{x_2}) = \int_{\Omega_1} \mathbf{G}(\mathbf{x}-\mathbf{x_2})\,d\mathbf{x} = \int_{\Omega_2} \mathbf{G}(\mathbf{x}_1-\mathbf{x})\,d\mathbf{x} \quad (26)$$

$$\mathbf{G}^2(\mathbf{x_1}-\mathbf{x_2}) = \frac{1}{\Omega}\int_{\Omega_1}\int_{\Omega_2} \mathbf{G}(\mathbf{x}-\mathbf{x}')\,d\mathbf{x}'d\mathbf{x} \quad (27)$$

2.3. Ensemble-volume averaged fields

Let us now consider the case that many equal-sized spherical inclusions distributed randomly in an elastic solid. Based on the solution of Equation 24, which represents the effect of pair-wise interaction, and assuming that no inclusion overlaps with each other, the ensemble-average solution of $\mathbf{d}^*$ within the context of approximate pairwise inter-inclusion interaction can be obtained by integrating $\mathbf{d}^*$ over all possible positions ($\mathbf{x}_2$) of the second inclusion for a given location of the first inclusion ($\mathbf{x}_1$). The ensemble-average process can be expressed as

$$\langle \mathbf{d}^* \rangle(\mathbf{x}_1) = \int_{V-\Omega_1} \mathbf{d}^*(\mathbf{x}_1-\mathbf{x}_2)P(\mathbf{x}_2 \mid \mathbf{x}_1)\,d\mathbf{x}_2 \quad (28)$$

where $P(\mathbf{x}_2 \mid \mathbf{x}_1)$ is the conditional probability function for finding the second inclusion centered at $\mathbf{x}_2$ given the first inclusion centered at $\mathbf{x}_1$. In addition, angled brackets denote the ensemble-average operator.

Finally, the approximate ensemble-volume averaged eigenstrain accounting for pairwise interaction in an inclusion, denoted as $\langle \bar{\boldsymbol{\epsilon}}^* \rangle$, can be expressed as follows [12]

$$\langle \bar{\boldsymbol{\epsilon}}^* \rangle = \boldsymbol{\Gamma}:\boldsymbol{\epsilon}^{*0} \quad (29)$$

where the components for the isotropic tensor $\boldsymbol{\Gamma}$ are defined as

$$\Gamma_{ijkl} = \gamma_1\delta_{ij}\delta_{kl} + \gamma_2(\delta_{ik}\delta_{jl} + \delta_{il}\delta_{jk}) \quad (30)$$

in which δ_{ij} is the Kronecker delta,

$$\gamma_1 = \frac{5\phi}{4\beta^2}\left\{-2(1-\nu_0) - 5\nu_0^2 - \frac{4\alpha}{3\alpha+2\beta}(1+\nu_0)(1-2\nu_0)\right\} \quad (31)$$

and

$$\gamma_2 = \frac{1}{2} + \frac{5\phi}{8\beta^2}\left\{11(1-\nu_0) + 5\nu_0^2 - \frac{3\alpha}{3\alpha+2\beta}(1+\nu_0)(1-2\nu_0)\right\} \quad (32)$$

where

$$\alpha = 2(5\nu_0-1) + 10(1-\nu_0)\left(\frac{\kappa_0}{\kappa_1-\kappa_0} - \frac{\mu_0}{\mu_1-\mu_0}\right) \quad (33)$$

$$\beta = 2(4-5\nu_0) + 15(1-\nu_0)\frac{\mu_0}{\mu_1-\mu_0} \quad (34)$$

In Equations 31 and 32, ϕ denotes the volume fraction of the inclusions in the composite material under consideration. In addition, ν, κ, and μ represent the Poisson's ratio, bulk modulus, and shear modulus, respectively, for the corresponding material phase which is denoted via the corresponding subscript. Subscript 0 is for the matrix phase and subscript 1 denotes the inclusion phase. For simplicity, both the matrix phase and the inclusion phase are assumed to be isotropic and the loading applied is within their elastic limits.

It is evident from Equation 29 that if the interaction tensor $\boldsymbol{\Gamma}$ is set to be equal to the identity $\mathbf{I}$, which means that, in indicial notation,

$$\Gamma_{ijkl} = I_{ijkl} = \frac{1}{2}(\delta_{ik}\delta_{jl} + \delta_{il}\delta_{jk}) \quad (35)$$

then, the formulation recovers the case where the effects of inter-inclusion interaction are neglected.

As illustrated in [12], the governing ensemble-volume averaged field equation relating the average strain $\bar{\boldsymbol{\epsilon}}$, the uniform remote strain $\boldsymbol{\epsilon}^0$, and the average

eigenstrain $\bar{\epsilon}^*$ can be expressed as:

$$\bar{\boldsymbol{\epsilon}} = \boldsymbol{\epsilon}^0 + \phi \mathbf{S} : \bar{\boldsymbol{\epsilon}}^* \tag{36}$$

With Equations 36, 29 and 17, we get

$$\bar{\boldsymbol{\epsilon}}^* = \mathbf{B} : \bar{\boldsymbol{\epsilon}} \tag{37}$$

where

$$\mathbf{B} = \boldsymbol{\Gamma} \cdot [-\mathbf{A} - \mathbf{S} + \phi \mathbf{S} \cdot \boldsymbol{\Gamma}]^{-1} \tag{38}$$

By taking the ensemble-volume average of the fundamental equation for the Eshelby's equivalence principle:

$$\mathbf{C}_1 : \boldsymbol{\epsilon}(\mathbf{x}) = \mathbf{C}_0 : \lfloor \boldsymbol{\epsilon}(\mathbf{x}) - \boldsymbol{\epsilon}^*(\mathbf{x}) \rfloor \tag{39}$$

the relationship between the local strain average and the eigenstrain average can be written as

$$\mathbf{C}_1 : \bar{\boldsymbol{\epsilon}}_1 = \mathbf{C}_0 : [\bar{\boldsymbol{\epsilon}}_1 - \bar{\boldsymbol{\epsilon}}^*] \tag{40}$$

Further utilizing Equation 18, we arrive at

$$\bar{\boldsymbol{\epsilon}}_1 = -\mathbf{A} : \bar{\boldsymbol{\epsilon}}^* \tag{41}$$

then, with Equation 37,

$$\bar{\boldsymbol{\epsilon}}_1 = -(\mathbf{A} \cdot \mathbf{B}) : \bar{\boldsymbol{\epsilon}} \tag{42}$$

Hence, upon comparing Equation 42 with Equation 8, the strain concentration factor tensor considering the effect of inter-inclusion interaction can be written as

$$\mathbf{A}_1 = -\mathbf{A} \cdot \mathbf{B} \tag{43}$$

The corresponding stress concentration factor tensor can be derived by using Equations 13 and 14. The explicit expression for the stress concentration factor tensor takes the following form

$$\mathbf{B}_1 = -\mathbf{C}_1 \cdot \mathbf{A} \cdot \mathbf{B} \cdot [\mathbf{I} - \phi \mathbf{B}]^{-1} \cdot \mathbf{C}_0^{-1} \tag{44}$$

Substituting Equation 43 into Equation 15 leads to the effective elastic stiffness tensor incorporating the effect of inter-inclusion interaction

$$\mathbf{C}_* = \mathbf{C}_0 \cdot \{\mathbf{I} - \phi \boldsymbol{\Gamma} \cdot (-\mathbf{A} - \mathbf{S} + \phi \mathbf{S} \cdot \boldsymbol{\Gamma})^{-1}\} \tag{45}$$

It is noted that Equation 45 recovers the results from the Mori-Tanaka method if the effect of inter-inclusion interaction is neglected, i.e., letting $\boldsymbol{\Gamma} \to \mathbf{I}$ or equivalently setting $\gamma_1 \to 0$ and $\gamma_2 \to \frac{1}{2}$.

2.4. Effective elastic moduli of porous materials

Since the pores are assumed to be distributed randomly among the matrix material, the porous material is statistically isotropic. Therefore, the effective elastic properties represented by the effective bulk modulus κ_* and the effective shear modulus μ_* can be explicitly written as

$$\kappa_* = \kappa_0 \left\{ 1 + \frac{30(1-\nu_0)\phi(3\gamma_1 + 2\gamma_2)}{3\alpha + 2\beta - 10(1+\nu_0)\phi(3\gamma_1 + 2\gamma_2)} \right\} \tag{46}$$

$$\mu_* = \mu_0 \left\{ 1 + \frac{30(1-\nu_0)\phi\gamma_2}{\beta - 4(4-5\nu_0)\phi\gamma_2} \right\} \tag{47}$$

In Equations 46 and 47, ϕ represents the porosity. For a porous material, $\kappa_1 = \mu_1 = 0$,

$$\alpha = 2(5\nu_0 - 1) \tag{48}$$

$$\beta = -7 + 5\nu_0 \tag{49}$$

and

$$\gamma_1 = \frac{\left(-12 + 18\nu_0 - 15\nu_0^2\right)\phi}{4(-7+5\nu_0)^2} \tag{50}$$

$$\gamma_2 = \frac{1}{2} + \frac{\left(107 - 98\nu_0 + 65\nu_0^2\right)\phi}{16(-7+5\nu_0)^2} \tag{51}$$

The scaled effective bulk modulus and effective shear modulus of a porous material can be expressed as

$$\frac{\kappa_*}{\kappa_0} = \frac{(1-2\nu_0)\{16(7-5\nu_0) - 2[8(7-5\nu_0) + 5(1+\nu_0)\phi]\phi\}}{16(1-2\nu_0)(7-5\nu_0) + (1+\nu_0)[8(7-5\nu_0) + 5(1+\nu_0)\phi]\phi} \tag{52}$$

$$\frac{\mu_*}{\mu_0} = \frac{(7-5\nu_0)\left\{8(7-5\nu_0)^2 - \phi\left[8(7-5\nu_0)^2 + \left(107 - 98\nu_0 + 65\nu_0^2\right)\phi\right]\right\}}{8(7-5\nu_0)^3 + 2(4-5\nu_0)\phi\left[8(7-5\nu_0)^2 + \left(107 - 98\nu_0 + 65\nu_0^2\right)\phi\right]} \tag{53}$$

The effective Young's modulus E_* and Poisson's ratio ν_* of a porous material are obtained through the following relations

$$E_* = \frac{9\kappa_*\mu_*}{3\kappa_* + \mu_*} \tag{54}$$

$$\nu_* = \frac{3\kappa_* - 2\mu_*}{2(3\kappa_* + \mu_*)} \tag{55}$$

If inter-pore interaction is neglected, the scaled elastic moduli can be easily obtained by setting $\gamma_1 \to 0$ and $\gamma_2 \to \frac{1}{2}$,

$$\frac{\kappa_*}{\kappa_0} = \frac{2(1-2\nu_0)(1-\phi)}{2(1-2\nu_0) + (1+\nu_0)\phi} \tag{56}$$

$$\frac{\mu_*}{\mu_0} = \frac{(7-5\nu_0)(1-\phi)}{7 - 5\nu_0 + 2(4-5\nu_0)\phi} \tag{57}$$

$$\frac{E_*}{E_0} = \frac{2(7-5\nu_0)(1-\phi)}{2(7-5\nu_0) + (1+\nu_0)(13-15\nu_0)\phi} \tag{58}$$

3. Results and discussion

3.1. Comparison with experimental results

There are a number of experimental results of the effective elastic properties for porous materials available in the literature. Here, the experimental data on Al_2O_3 [13], porous glass [14], Gd_2O_3 [15], Sm_2O_3 [16], which have representative matrix Poisson's ratios equal to 0.19, 0.23, 0.277 and 0.3245, respectively, are chosen to be compared with the predictions from the proposed model.

The predicted results of the scaled Young's modulus, E_*/E_0, and the scaled shear modulus, μ_*/μ_0 for porous alumina (Al_2O_3) are presented in Figs 2 and 3. The elastic moduli of the matrix material: $E_0 = 386$ GPa, $\mu_0 = 163$ GPa and $\nu_0 = 0.19$ are used as input. The comparison with the experimental data of Coble and Kingery [13] is also included in Figs 2 and 3. It is evident from these figures that there is an excellent agreement between the predictions and the experimental values.

The experimental results for the effective bulk modulus of porous glass as a function of porosity were presented in [14]. Fig. 4 shows the comparison between these experimental data and the predictions from the proposed model. An excellent agreement between the predictions and the measured data can be observed.

Figs 5 and 6 show the predicted scaled effective elastic moduli of polycrystalline monoclinic Gd_2O_3 using $E_0 = 150.26$ GPa, $\mu_0 = 58.85$ GPa and $\nu_0 = 0.277$ as input. The experimental data of Haglund and Hunter [15] are also presented in Figs 5 and 6. It is noted that the predictions agree very well with the experimental data up to $\phi = 0.23$.

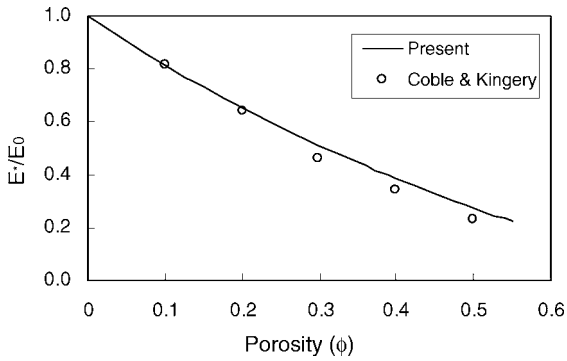

Figure 2 Scaled effective Young's modulus for porous Al_2O_3 ($E_0 =$ 386 GPa, $\mu_0 = 163$ GPa).

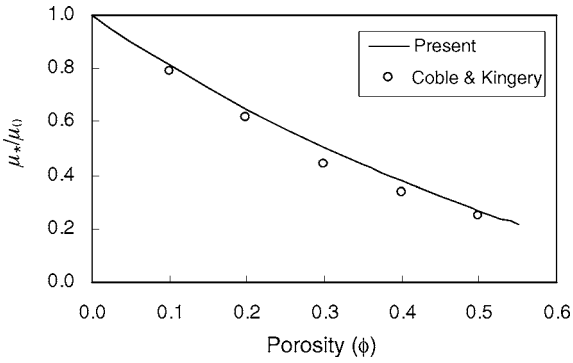

Figure 3 Scaled effective shear modulus for porous Al_2O_3 ($E_0 =$ 386 GPa, $\mu_0 = 163$ GPa).

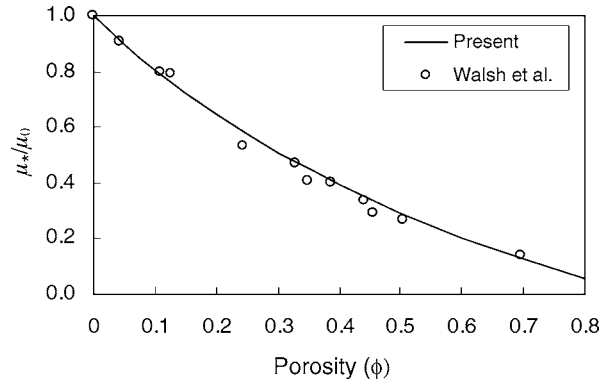

Figure 4 Scaled effective bulk modulus for porous glass ($\kappa_0 = 46$ GPa, $\nu_0 = 0.23$).

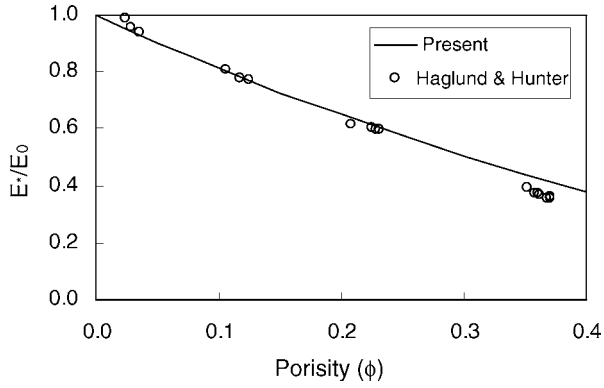

Figure 5 Scaled effective Young's modulus for Gd_2O_3 ($E_0 =$ 150.26 GPa, $\mu_0 = 58.85$ GPa).

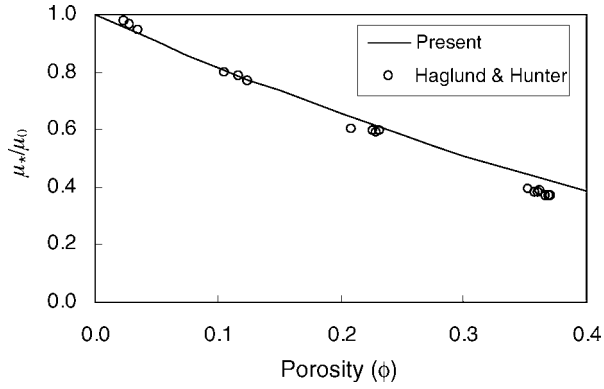

Figure 6 Scaled effective shear modulus for Gd_2O_3 ($E_0 = 150.26$ GPa, $\mu_0 = 58.85$ GPa).

The comparisons of the scaled effective elastic properties as a function of porosity for polycrystalline monoclinic Sm_2O_3 [16] are shown in Figs 7 and 8. A very good agreement for small porosity (<0.1) is noted. When $\phi \geq 0.1$, the predictions are slightly higher than the measured values.

3.2. Comparison with other theoretical models

Several different theoretical models have been developed to predict the effective elastic moduli for porous materials. Ramakrishnan and Arunachalam [17] presented a detailed summary of these models. Here, the predictions from the proposed model are compared with the results calculated from the following

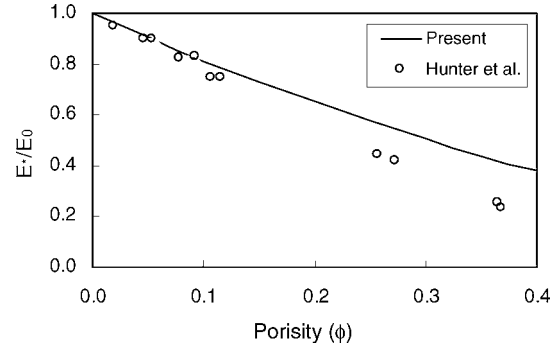

Figure 7 Scaled effective Young's modulus for porous Sm_2O_3 ($E_0 = 145$ GPa, $\mu_0 = 54.75$ GPa).

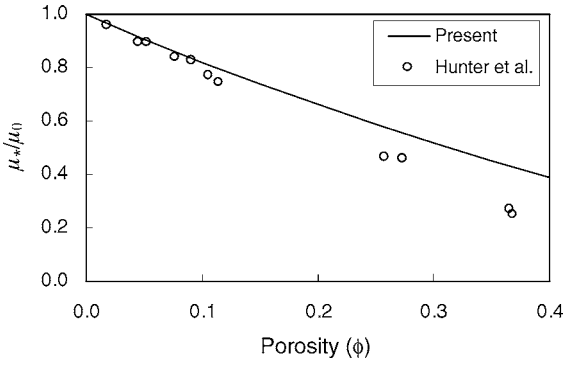

Figure 8 Scaled effective shear modulus for porous Sm_2O_3 ($E_0 = 145$ GPa, $\mu_0 = 54.75$ GPa).

well-known theoretical models: the composite sphere model (CSM), the self-consistent method (SCM), the differential method (DM), the generalized method of cells (GMC), and the unit cell finite element method (UCFEM).

In the composite sphere model [18, 19], the two-phase porous material is approximated as an assemblage of different-sized composite sphere that consists of a sphere of matrix material and a second concentrically inside spherical phase. When this model is extended to a porous material, the effective bulk modulus is expressed as

$$\frac{\kappa_*}{\kappa_0} = \frac{2(1-2\nu_0)(1-\phi)}{2(1-2\nu_0)+(1+\nu_0)\phi} \tag{59}$$

The bounds on Young's modulus and shear modulus are written as

$$0 \le \frac{E_*}{E_0} \le \frac{2(7-5\nu_0)(1-\phi)}{2(7-5\nu_0)+(1+\nu_0)(13-15\nu_0)\phi} \tag{60}$$

$$0 \le \frac{\mu_*}{\mu_0} \le \frac{(7-5\nu_0)(1-\phi)}{7-5\nu_0+2(4-5\nu_0)\phi} \tag{61}$$

It is shown that the upper bounds of Hashin's equations are identical to those presented equations for the non-interacting case. This is because these presented equations recover the results from the Mori-Tanaka method [6], which coincides with the Hashin's upper bounds as pointed out by Ramakrishnan and Arunachalam [17].

Ramakrishnan and Arunachalam [17] presented a modified composite sphere model, and their equations

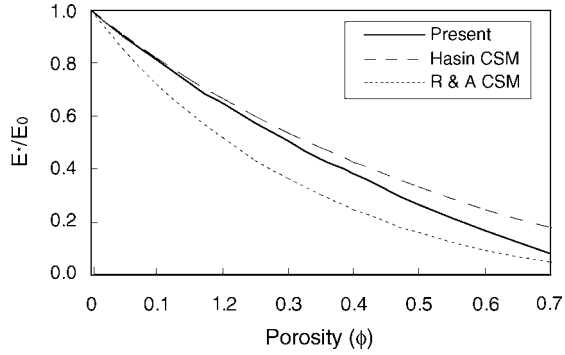

Figure 9 Scaled Young's modulus predicted from proposed model and composite sphere models.

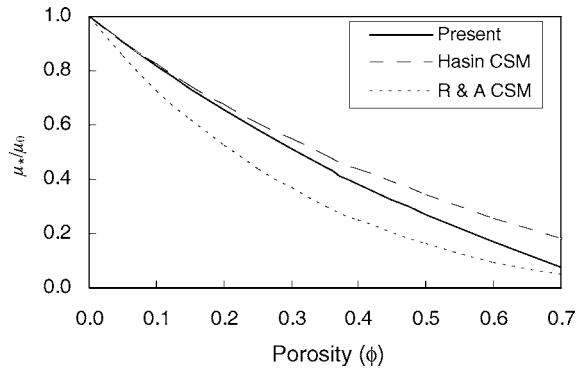

Figure 10 Scaled shear modulus predicted from proposed model and composite sphere models.

for the effective elastic moduli are given by

$$\frac{E_*}{E_0} = \frac{(1-\phi)^2}{1+(2-3\nu_0)\phi} \tag{62}$$

$$\frac{\mu_*}{\mu_0} = \frac{4(1+\nu_0)(1-\phi)^2}{4(1+\nu_0)+(11-19\nu_0)\phi} \tag{63}$$

Figs 9 and 10 show the comparison for the scaled Young's modulus and the shear modulus predicted by the proposed model, the composite sphere model [18] and the modified composite sphere model [17]. The elastic properties: $E_0 = 150.26$ GPa, $\mu_0 = 58.85$ GPa and $\nu_0 = 0.277$ [15], are used. From Figs 9 and 10, the predictions from the proposed model show similar trends as compared to the other models and lie between the curves for the upper bound of the Hashin model and the Ramakrishnan-Arunchalam model. The proposed model correlates very well with the experimental results (Figs 5 and 6), suggesting that the Ramakrishnan-Arunachalam model considerably underestimates the effective elastic moduli of Gd_2O_3.

In the self-consistent method [3, 4], the effects of inclusion interaction are approximated by embedding a spherical inclusion in a matrix of unknown effective moduli. For porous materials, the Hill-Budiansky's equation for the shear modulus could be expressed as

$$\left(\frac{\mu_*}{\mu_0}\right)^2 + \left\{\frac{(1+\nu_0)(3-\phi)}{4(1-2\nu_0)} + \frac{(5\phi-2)}{2}\right\}\left(\frac{\mu_*}{\mu_0}\right) + \frac{3(1+\nu_0)(2\phi-1)}{4(1-2\nu_0)} = 0 \tag{64}$$

The bulk modulus is given as

$$\frac{\kappa_*}{\kappa_0} = \frac{2(1-2\nu_0)(1-\phi)}{2(1-2\nu_0)+(1+\nu_0)\phi\left(\frac{\mu_*}{\mu_0}\right)} \tag{65}$$

Zimmerman [5] used the differential method and established the following equations for the elastic moduli of porous material [17]

$$\frac{\mu_*}{\mu_0} = \frac{(1-\phi)^2}{3(1-\nu_0)}\left[2(1+\nu_0)+(1-5\nu_0)\left(\frac{\mu_*}{\mu_0}\right)^{3/5}\right]^{1/3} \tag{66}$$

$$\frac{\kappa_*}{\kappa_0} = \frac{2(1-2\nu_0)\left(\frac{\mu_*}{\mu_0}\right)}{(1+\nu_0)+(1-5\nu_0)\left(\frac{\mu_*}{\mu_0}\right)^{3/5}} \tag{67}$$

Comparisons of the predictions for the scaled Young's modulus and the shear modulus from the proposed model, the self-consistent method [3, 4] and the differential method [5] are presented in Figs 11 and 12. The elastic properties of Gd_2O_3: $E_0 = 150.26$ GPa, $\mu_0 = 58.85$ GPa and $\nu_0 = 0.277$ [15], are used as input. It is observed from these figures that the proposed model agrees with the Zimmerman model.

Herakovich and Baxter [8] used the generalized method of cells to determine the effective elastic properties of porous materials for four distinct pore shapes: cylinder, cube, sphere and cross. In Roberts and Garboczi [1], the finite element method was employed

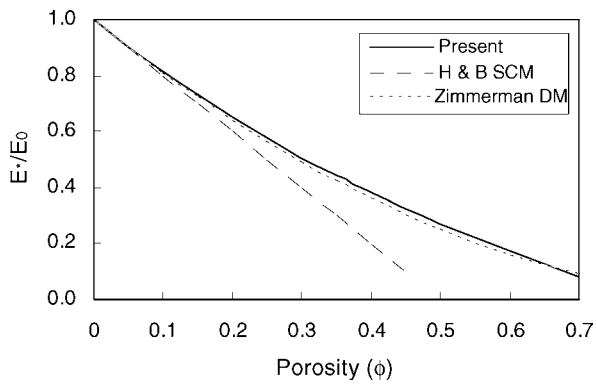

Figure 11 Comparison of Young's modulus with self-consistent method and differential method.

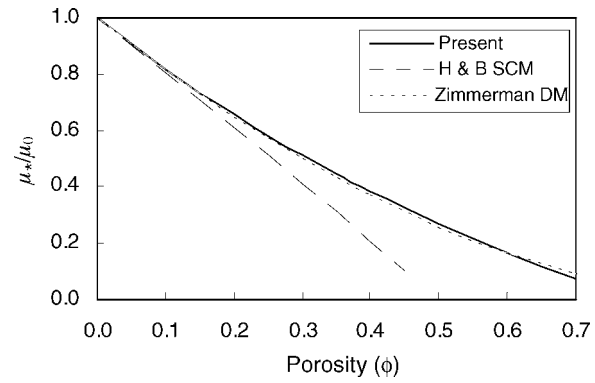

Figure 12 Comparison of shear modulus with self-consistent method and differential method.

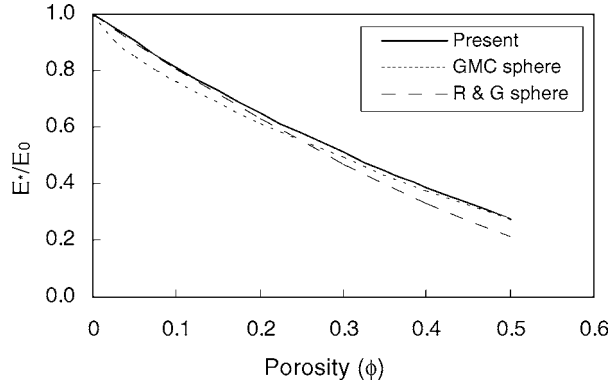

Figure 13 Comparison of Young's modulus with GMC sphere model and R&G sphere model.

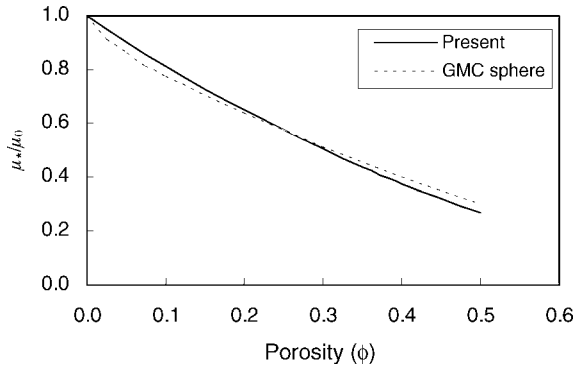

Figure 14 Comparison of shear modulus with GMC sphere model.

to derive formulas that relate the elastic properties of ceramics to porosity and microstructure for three different models: spherical pores, solid spheres, and ellipsoidal pores. Figs 13 and 14 present the comparisons for the scaled Young's modulus and shear modulus predicted by the proposed model, the GMC sphere model [8] and the Roberts-Garboczi model [1]. The elastic moduli of Al_2O_3: $E_0 = 386$ GPa, $\mu_0 = 163$ GPa and $\nu_0 = 0.19$ [13], are used. It is shown from these figures that the proposed model, the GMC sphere model and the Roberts-Garboczi model are in good agreement. For low porosity of $\phi \leq 0.2$, the proposed model correlates better with the Roberts-Garboczi model, and for $\phi > 0.2$, the proposed model agrees more closely with the GMC sphere model.

3.3. Poisson ratio

The effective Poisson's ratios as a function of porosity and ν_0 are presented in Fig. 15 for low to intermediate porosity. Both interaction and non-interaction cases are included. If the inter-pore interaction is considered, increase in porosity leads to a decrease in the effective Poisson's ratio for ν_0 above 0.25, and causes the effective Poisson's ratio to increase for ν_0 below 0.25. If the inter-pore interaction is neglected, the effective Poisson's ratio will decrease with increasing porosity for ν_0 higher than 0.2, and increases as porosity increases for ν_0 less than 0.2. For low porosity, the difference in Poisson's ratio for the interaction and non-interaction is negligible, but this difference increases with increasing porosity.

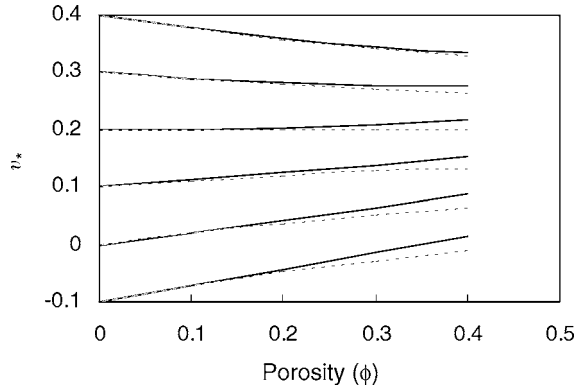

Figure 15 Effective Poisson's ratio as a function of porosity and ν_0. Solid lines consider inter-pore interaction and dashed lines neglect inter-pore interaction.

4. Conclusions

A statistical micromechanical approach is presented in this paper to predict the effective elastic properties of porous materials based on the theory of average fields, the proposed approximate pairwise interaction solutions and the ensemble-volume averaging process. Closed-form and analytical explicit expressions for the effective elastic moduli have been derived in terms of the mechanical properties of the matrix material and porosity. The present formulation differs from most of existing theoretical methods in that the interaction effects among the pores are directly accounted for through taking the statistical average on the solution of the pairwise inter-inclusion interaction problem.

It is shown in Section 3 that the predicted effective elastic moduli are in good agreement with several sets of previously published experimental data reported by Coble and Kingery [13], Walsh *et al*. [14], Haglund and Hunter [15], Hunter *et al.* [16]. Comparisons with several other existing theoretical models have shown that the present model, the Zimmermon's differential method, the GMC sphere model and the Roberts-Garboczi's model are in good agreement. In Sections 2 and 3, it is explicitly demonstrated that the presented formulation recovers the classical Hashin bounds and the Mori-Tanaka estimates if the effects of the inter-pore interaction are neglected. The dependence of the effective Poisson's ratio on the porosity is also investigated.

The presented method can be readily modified to accommodate pores of different sizes. The proposed micromechanical framework provides a new approach for analytical estimation of effective properties of linear porous materials. No parameter estimation or data fitting is required in the proposed framework.

References

1. A. P. ROBERTS and E. J. GARBOCZI, *J. Amer. Ceram. Soc.* **83**(12) (2000) 3041.
2. M. A. QIDWAI, P. B. ENTCHEV, D. C. LAGOUDAS and V. G. DeGIORGI, *Int. J. Solids and Struc.* **38** (2001) 8653.
3. R. HILL, *J. Mech. and Phys. Solids* **13**(4) (1965) 213.
4. B. BUDIANSKY, *ibid.* **13**(4) (1965) 223.
5. R. W. ZIMMERMAN, *Mech. Mater.* **12** (1991) 17.
6. T. MORI and K. TANAKA, *Acta Metallurgica* **21**(5) (1973) 571.
7. R. W. RICE, *J. Mater. Sci.* **31** (1996) 1509.
8. C. T. HERAKOVICH and S. C. BAXTER, *ibid.* **31** (1999) 1595.
9. R. HILL, *J. Mech. and Phys. Solids* **48** (1963) 367.
10. G. J. DVORAK, in "Metal Matrix Composites: Mechanisms and Properties," edited by R. K. Everett and R. J. Arsenault (Academic Press, Boston, USA, 1991).
11. T. MURA, "Micromechanics of Defects in Solids," 2nd ed. (Kluwer Academic Publishers, 1987).
12. K. H. TSENG, Ph.D. Dissertation, Princeton University, Princeton, New Jersey, 1995.
13. R. L. COBLE and W. D. KINGERY, *J. Amer. Ceram. Soc.* **39**(11) (1956) 377.
14. J. B. WALSH, W. F. BRACE and A. W. ENGLAND, *ibid.* **48**(12) (1965) 605.
15. J. A. HAGLUND and O. HUNTER, *ibid.* **56**(6) (1973) 327.
16. O. HUNTER, H. J. KORKLAN and R. R. SUCHOMEL, *ibid.* **57**(6) (1974) 267.
17. N. RAMAKRISHNAN and V. S. ARUNACHALAM, *ibid.* **76**(11) (1993) 2745.
18. Z. HASHIN, *J. Appl. Mech.* **29** (1962) 143.
19. Z. HASHIN and S. SHTRIKMAN, *J. Mech. Phys. Solids* **11** (1963) 127.

Received 12 December 2002
and accepted 14 May 2003